Nanotechnology

Novel insight on the local surface properties of ZnO nanowires

To cite this article before publication: Monika Kwoka *et al* 2020 *Nanotechnology* in press https://doi.org/10.1088/1361-6528/ab8dec

IOP Publishing Journal Title
Journal **XX** (XXXX) XXXXXX https://doi.org/XXXX/XXXX

Novel insight on the local surface properties of ZnO nanowires

Monika Kwoka [1]*, Anna Kulis-Kapuscinska[1], Dario Zappa [2], Elisabetta Comini [2] , Jacek Szuber [1]

[1] Department of Cybernetics, Nanotechnology and Data Processing, Faculty of Automatic Control, Electronics and Computer Science, Silesian University of Technology, 44-100 Gliwice, Poland
[2] SENSOR Lab, Department of Information Engineering (DII), Brescia University, 25123 Brescia, Italy

***E-mail: monika.kwoka@polsl.pl**

Received xxxxxx
Accepted for publication xxxxxx
Published xxxxxx

Abstract

Novel insight on the local surface properties of ZnO nanowires (NW) deposited by the evaporation-condensation method on Ag-covered Si substrates is proposed, based on the results of comparative studies by using the Scanning Electron Microscopy (SEM), X-ray photoemission spectroscopy (XPS) and Thermal Desorption Spectroscopy (TDS) methods, respectively. SEM studies showed that ZnO nanowires (nanoribbons) are mostly isolated and irregular, having the average length μm and the average at the level of tens nm, respectively. Our XPS studies confirmed their evident surface non-stoichiometry, combined with strong C surface contaminations, which was related to the existence of oxygen-deficient regions. Additionally, TDS studies showed that undesired surface contaminations (including C species and hydroxyl groups) on the surface of ZnO NWs can be removed almost completely, leading to an increase of the final non-stoichiometry. Both effects are of great importance when using ZnO NWs for the detection of oxidizing gases, because the undesired C contaminations (including C-OH species) play the role of undesired barriers for the gas adsorption, especially at the low working temperature, additionally affecting the uncontrolled sensor ageing effect.

Keywords: ZnO nanowires; surface morphology; SEM; surface chemistry; XPS; surface reactivity; TDS

Introduction

Zinc oxide (ZnO) is one of the most popular transparent conductive oxides (TCO), having unique optical properties (wide band gap of 3.37 eV, and large exciton binding energy (60 meV)) as well as electronic properties (high electronic mobility up to 2 $cm^2/V \cdot s$). It has a widespread application, mainly in optoelectronics and photovoltaics [1-4]. In addition, due to the above mentioned high mobility of conduction electrons and good chemical and thermal stability, recently ZnO became one of the most interesting and very promising gas sensing material [5,6].

It should be noted that already in 90s Sberveglieri et al. [7], as well as other researchers, have shown that ZnO thin films are very useful for the detection of oxygen. However, even after many years of exploring fundamental sensing parameters, including the response and recovery times, the undesired ageing effect of oxide semiconductors, including ZnO, remains mostly unknown. This is related to the fact that the gas sensing effect appears within the surface space-charge region of sensor material, i.e. at the depth related to Debye length, after its exposure to gas, in this region, the surface state density of sensor material is balanced by acceptors and donors, creating a surface band bending [8].

In the last few years, it was a commonly accepted idea that the gas sensing performance of a sensor material (including ZnO) can be improved mainly by its manufacturing in the form of nanostructures. The nanosized materials exhibit, among others, a high-density of active surface sites, a large specific surface (defined as surface-to-volume ratios) compared with their bulk counterparts, quantum-sized effects, as well as an efficient transport of electrons and excitons. In general, these properties can be achieved also by the three-dimensional (3D) ZnO nanostructures, in the form of thin films [9,10,11], nanoflowers [12-16], hollow spheres [17-19] and nanoflakes [20,21]. Nevertheless, quasi one-dimensional (1D) nano-forms of ZnO, like nanowires [22-27], nanorods [28-32] and

nanobelts [33,34], are very promising for potential gas sensors applications. The preparation and characterization of those ZnO quasi one-dimensional (1D) nanoforms for potential gas sensor applications were nicely reviewed in literature [5,6,35-41].

What is crucial, during the gas sensing effects, is that surface adsorption/chemisorption processes of gaseous species take place mainly at the surface of crystalline ZnO nanowires. These processes are responsible for the charges redistribution within the surface space-charge region of sensor material and the appearance of surface bend bending effect [42]. For the ZnO nanowires, the charge carrier concentration reaches the value of $\sim 10^{18}$ [cm^{-3}], and a surface depletion region (upward band bending) is usually observed [23], which is directly responsible for the specific surface conduction mechanism. In some cases, the transverse dimension of ZnO nanowires (NWs) can be even smaller than 10 nm. This dimension is comparable to the Debye length, therefore in such a case one can expect the highest detection efficiency of gas molecules adsorbed at their surface.

Having all above in mind, it is evident that the detailed information on ZnO NWs surface chemistry is absolutely indispensable for the deep understanding of gas sensing mechanism, allowing the design and construction of novel gas sensor devices based on this material.

X-ray photoemission spectroscopy (XPS) is considered one of the best technique for monitoring the surface chemistry of ZnO NWs, including stoichiometry and undesired surface contaminations. In one of our [43], preliminary XPS studies on ZnO NWs exhibited an evident nonstoichiometry with oxygen deficiencies, even before thermal annealing under UHV conditions. In turn, in our subsequent [44], XPS method was applied for the monitoring of the surface chemistry of ZnO nanowires gas sensors functionalized by chemical modification, allowing an enhancement of NO_2 gas sensor response. This technique was also applied in our recent study for the control of the surface chemistry of nanostructured ZnO thin films deposited by the direct current (DC) reactive magnetron sputtering (DCRMS) method [45].

In this paper, we surface properties of ZnO nanowires deposited the Ag-covered Si substrate obtained by using three comparative techniques, i.e. SEM method for the observation of their surface morphology, XPS method for the determination of their local surface nonstoichiometry and contaminations, TDS method for the control of surface active gases adsorbed at the surface of ZnO NW.

Experimental

Deposition of ZnO nanowires

ZnO nanowires (NW) were deposited on Si(100) substrates at SENSOR Lab, Department of Information Engineering, Brescia University, Italy, using an evaporation-condensation process in a custom furnace. ZnO powder was placed in the middle of furnace at high temperature (1370 °C) and condensed in a colder region (≈ 700 °C) where the substrates were placed. An inert gas flow (Ar, 100 sccm) was used to move the evaporated material toward the colder region of the furnace. Pressure was fixed at 100 mbar, and it was controlled finely by barometer (MKS, Germany). In order to reach a good uniformity of the ZnO NWs lateral dimensions, a catalyzed-assisted growth has been performed by Ag nanoparticles deposited onto the Si(100) substrates by DC magnetron sputtering (MS) method (Kenotec, Italy).

Surface characterization of ZnO nanowires

For the characterization surface properties of the ZnO NWs, a combination of SEM, XPS and TDS experiments were performed.

The surface morphology studies of ZnO NWs were carried out at SENSOR Lab, Brescia University, Italy, using a Field Emission Scanning Electron Microscope (FE-SEM, Gemini, Leo 1525) operated in the 3-5 keV range.

The surface stoichiometry of ZnO NWs, together with the presence of surface contaminations, was determined by using the XPS method, before and after the subsequent TDS experiments, respectively. For XPS analysis we used a commercial XPS spectrometer (SPECS, Germany) equipped with a X-ray lamp (AlK_α 1486.6 eV; XR-50 model), and a concentric hemispherical analyzer (PHOIBOS-100 Model). The XPS experiment have been performed at the background working pressure of ~ 10^{-7} Pa. The registered XPS spectra have been calibrated with respect to reference binding energies (BE) using both the XPS Au4f peak at 84.5 eV of an Au foil located on the sample holder, as well as the XPS C1s peak at 284.5 eV of residual C contamination always present on the surface of investigated ZnO nanowires.

The specific active surface gases desorbed from the surface of ZnO NWs were detected by the TDS method during a linear growth of the sample temperature (temperature programmable desorption – TPD), using the in line mass spectrometry (MS). TDS measurements have been performed in a sample preparation chamber equipped with a resistive type sample heating unit, combined with a temperature programmable control unit (OmniVac–Dual Regulated Power Supply PSReg120 model) and mass spectrometer - residual gas analyzer (Stanford RGA200 Model). During every TPD cycle in the temperature range of 50 ÷ 300°C, the typical gas sensor working conditions, the TDS spectra of selected gases like H_2, H_2O, O_2, and CO_2 have been registered.

Both XPS and TDS experiments have been performed at the Silesian University of Technology, Gliwice, Poland. Other experimental details have been described elsewhere [46-48].

Results and discussion

At the beginning of our studies we have focused on the surface morphology of ZnO NWs deposited on top of Ag-covered Si substrate and their SEM images at two different magnification levels and lateral resolutions are illustrated on Figure 1.

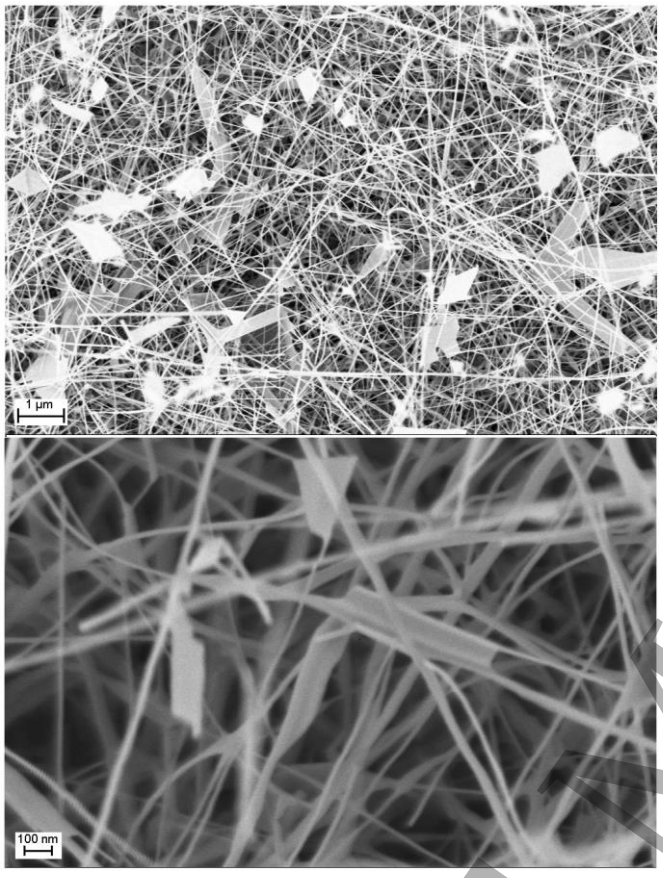

Figure 1. The SEM images of ZnO nanowires deposited on the Ag-covered Si(100) substrate at two different magnification levels.

It is clearly visible that the Ag-covered Si(100) substrate is covered completely by ZnO nanowires (nanoribbons) originating from the Ag metallic nanograins, contributing to the ZnO NWs nucleation growth process. The morphology of the nanowires is more visible in the SEM image at the higher magnification, which confirm that nanowires are mostly isolated and irregular, having various length exceeding one µm, as well as a various diameter (in the range of 10 ÷ 50 nm). This is crucial, having in mind that the gas sensor effect appears within the surface space-charge region of ZnO related to Debye length, which is in the range of several nm.

Afterwards, in to the morphological information above, we have focused on the surface chemistry of ZnO NWs deposited on Ag-covered Si substrate, with a special emphasis on the determination of its variation during the complementary thermal desorption experiments.

The survey spectra for ZnO NWs deposited at Ag-covered Si substrate before and after TPD process in the full binding energy (BE) range 0-1200 eV are presented in Figure 2 where apart from the typical Auger electron lines Zn LMM and O KLL peaks (not labelled - skipped), one can recognize the contribution of ZnO basic elements thanks to the presence of core level lines: Zn2p, O1s, Zn3s, Zn3p and Zn3d. Moreover, what is a crucial point of our XPS studies, an evident contribution of an undesired carbon contamination at the ZnO NWs surface was observed, as confirmed by the presence of XPS C1s lines at BE ~ 286.0 eV.

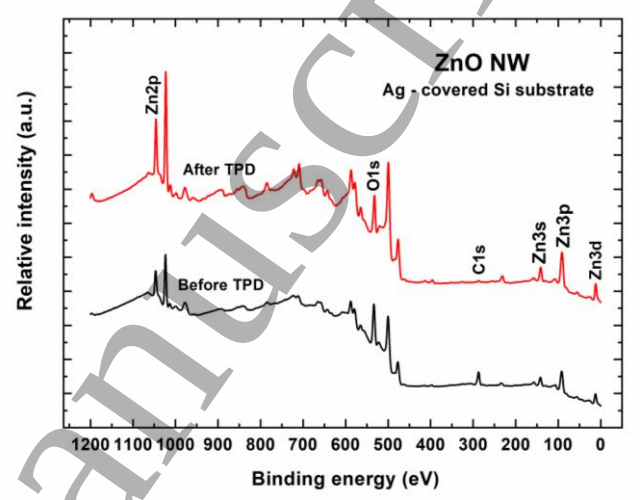

Figure 2. The evolution of XPS survey spectra of ZnO NWs before and after TPD process in a full 1200 eV binding energy range.

Considering the relative intensity (height) of $Zn2p_{3/2}$, O1s, and C1s XPS core level lines corrected by their respective atomic sensitivity factors (ASF), the relative concentration of the basic elements like O, Zn and C with respect to all atoms in the subsurface region can be calculated, according to the commonly used analytical procedure [49,50]. However, due to the high undesired background in the observed XPS survey spectra in the full binding energy range (1200 eV) and the contribution of Auger electron emission lines, the relative concentrations of the main elements of ZnO NWs have been calculated on the base of relative intensity of XPS core level lines in a limited range (600 eV) additionally corrected by the transmission function T(E) of CHA PHOIBOS 100 energy analyzer. The obtained data are summarized of **Table 1**.

Table 1. The relative concentration of basic elements O, Zn and C with respect to all the atoms in the subsurface region of ZnO NW based on the height of O1s, C1s and Zn3p XPS peaks.

ZnO NW	Relative concentration of main elements		
	[O]/ ([Zn]+[O]+[C])	[Zn]/ ([Zn]+[O]+[C])	[C]/ ([Zn]+[O]+[C])
Before TPD	0.35	0.32	0.33
After TPD	0.37	0.58	0.05

These respective values summarized in Table 1 directly correspond to a total relative concentration (in %) of basic elements i.e. O, Zn and C in subsurface region of ZnO NWs.

On the base of above summarized information, that before TPD process the contribution of main elements in the ZnO NWs surface/subsurface region is quite similar (~0.33). This is quite expected and a crucial information for their potential use as gas sensors because it is well known that hydrocarbon contamination is common on the air-exposed samples during sample handling or preparation [50]. Although the ZnO NWs exhibit almost stoichiometric form, after their exposure to air the undesired surface C contaminations can play a specific barrier for the gas interaction with expected surface sites waiting for the gas adsorption. In turn, after TPD process the contribution of main elements in the surface/subsurface region of ZnO NWs drastically changed. A first information is that after TPD process the contribution of undesired C contaminations drastically decreased, even reaching the noise level. In parallel, the relative O concentration with respect to all atoms in the subsurface region also drastically changed, reaching a value very far from the natural stoichiometry. Probably, this is related to the existence of specific forms of surface bondings for the main elements in the subsurface region of the analysed samples. Therefore the deeper analysis of the evolution of XPS Zn2p, O1s, and C1s lines related to main surface elements at ZnO NWs surface before and after TPD process has been performed.

The XPS Zn2p lines reveal two broadly resolved features at the binding energy of about 1045 eV and 1022 eV, which can be ascribed to the $Zn2p_{1/2}$ and $Zn2p_{3/2}$ for both samples, respectively as visible in Figure 3. This is related to the spin orbit splitting of ~ 23.0 eV, what is in a good agreement with available literature [48,51,52]. XPS spectra confirm that Zn element exists mainly in the form of Zn^{2+} on the ZnO NWs surfaces, corresponding to Zn atoms in the ZnO lattice [48,53].

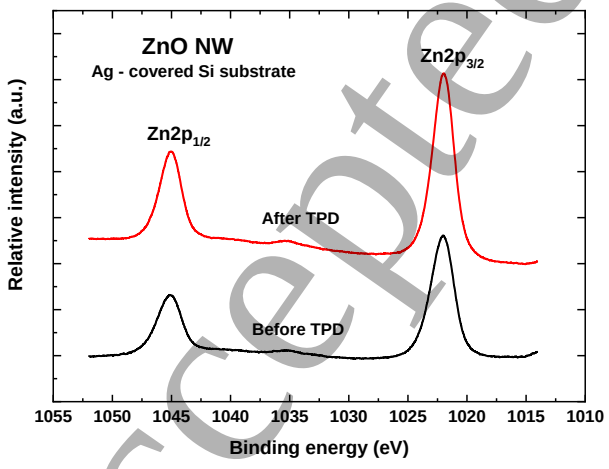

Figure 3. The evolution of XPS Zn2p core level lines ZnO NWs before and after TPD process.

However, it is clearly visible that XPS $Zn2p_{3/2}$ line is slightly asymmetrical. A precise deconvolution procedure has been performed for these lines the obtained results are shown in **Figure 4.**

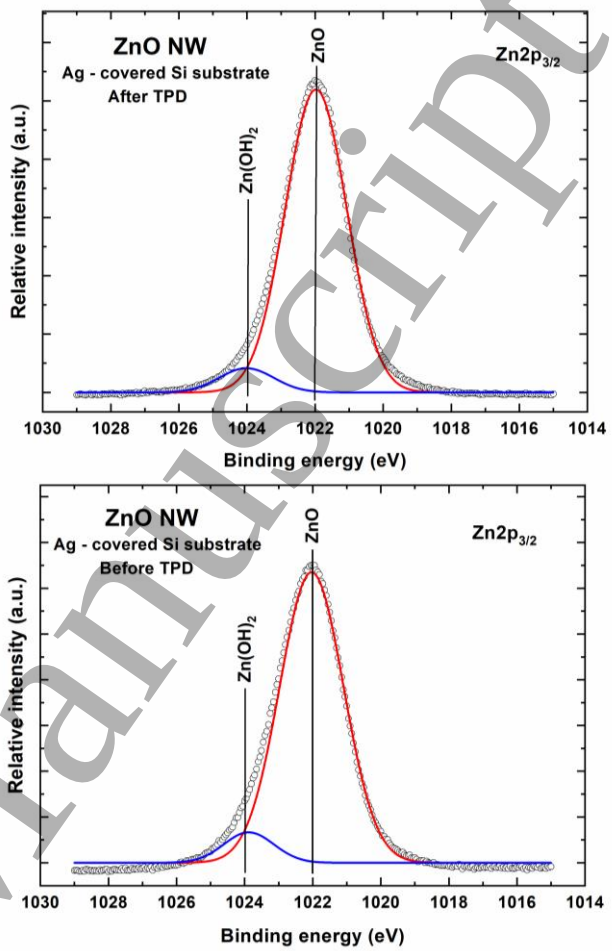

Figure 4. The XPS $2p_{3/2}$ lines for ZnO NWs before (lower) and after TPD process (upper) after deconvolution using Gauss fitting (dark circles - experimental spectra; colour solid lines - respective fitted components).

The deconvolution of $Zn2p_{3/2}$ lines exhibits two peaks located at binding energy ~1022.0 eV and at ~1024.0 eV, respectively, with very high line fitting (RMS = 0.995). The first one can be ascribed to the Zn atoms in the ZnO lattice [50]. In turn, the second one can be ascribed to the same zinc hydroxide $Zn(OH)_2$ species also observed for the ZnO nanoparticles by Guo et al. [54], and for the ZnO thin films by Armelao et al. [55]. The existence of specific $Zn(OH)_2$ on the surface of ZnO NWs before and after TPD process was also observed in the XPS O1s spectral lines what is demonstrated on Figure 5. Unlike XPS $Zn2p_{3/2}$ lines, the XPS O1s lines exhibit an evident asymmetry with two main parts, which are probably related to the existence of different forms of oxygen bondings at their surface. For their detailed verification, the deconvolution of XPS O1s lines was performed using the Gauss fitting. The obtained results are shown in Figure 6.

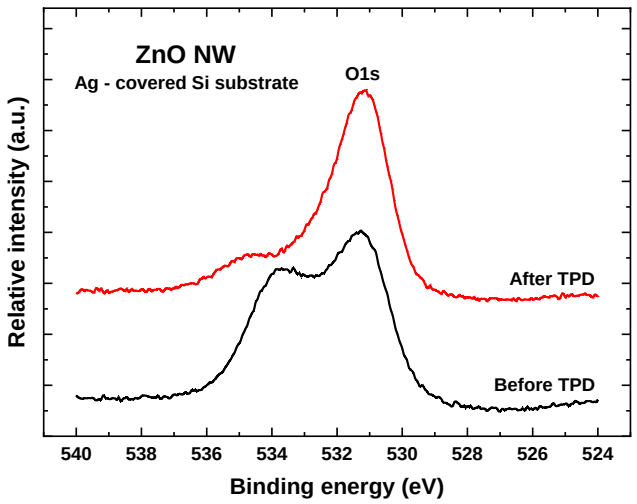

Figure 5. The evolution of XPS O1s core level lines of ZnO NWs before and after TPD process.

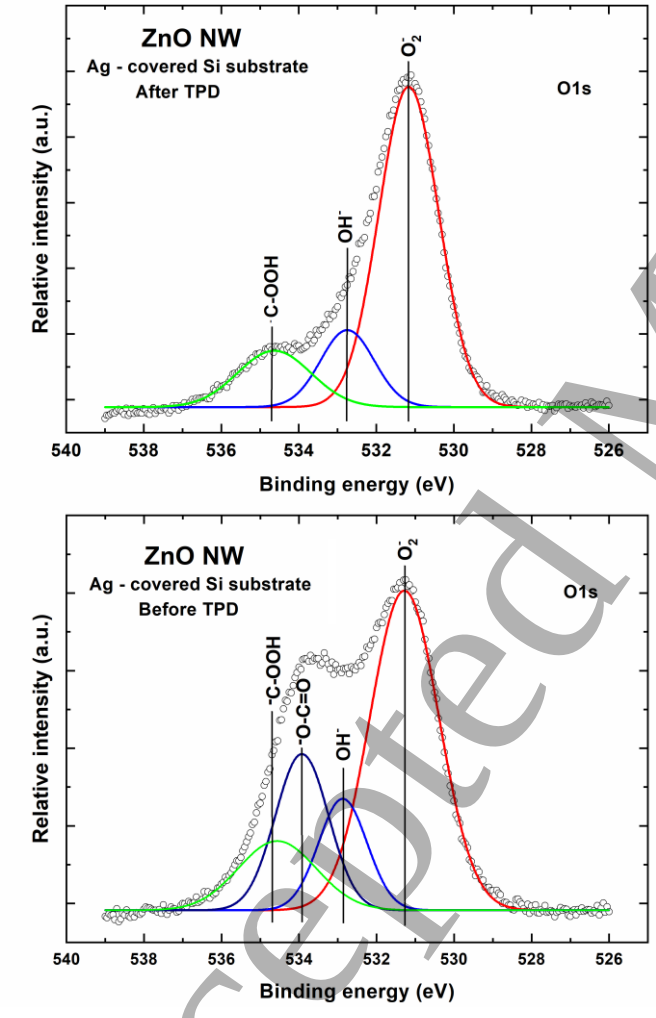

Figure 6. The XPS O1s lines for ZnO NWs before (lower) and after the TPD process (upper) after deconvolution using Gauss fitting (dark circles – experimental spectra; colour solid lines – respective fitted components).

In the case of ZnO NWs before TPD process, after the deconvolution procedure the XPS O1s line exhibits four components clearly visible at the binding energy of 531.2 eV, 532.8 eV, 533.9 eV and 534.6 eV, respectively.

The first one, which can be treated as the main peak located at 531.2 eV, can only be attributed to the presence of partially reduced ZnO such as ZnO_x direcly related to the existence of O_2^- ions caused by oxygen deficiencies within the ZnO matrix. This is extremely important information because its binding energy is about 1 eV higher with respect to the commonly observed O_2^- ions in the ZnO wurzite structure of the hexagonal Zn ion array (~ 530 eV) [49]. A similar peak located at 531.2 eV was observed, among others, by Chen et al. [56], Kaneva et al. [57] and Li et al. [58] for various ZnO thin films, as well as by Chen et al. [59] for the flower-like and tube-like ZnO nanomaterials. The existence of oxygen-deficient regions at the surface of ZnO NWs is of great importance because they can be responsible for the intrinsic sensing characteristic of ZnO, originating from the native defects (i.e. nonstoichiometry) such as oxygen vacancies and zinc interstitials. These defects are mainly located in the surface region and determine the electrical conductance, in particular in the quasi-mono dimensional structure of ZnO NWs with a large surface-to-volume ratio, having a great impact on the gas sensing characteristics of gas sensor systems and devices.

In turn, a second component of XPS O1s line located at 532.8 eV, evidently lower in intensity, can be attributed to the presence of loosely bounded oxygen on the surface of ZnO belonging to specific species, such as adsorbed H_2O, as well as adsorbed hydroxyl groups. A similar component was recently observed for ZnO thin films by Armelao et al. [55], Hsieh et al. [60], Lupan et al. [61], Stambolova et al. [62], as well as for low dimensional ZnO nanostructures by Guo et al. [54], Lee et al. [63], Bai et al. [64], Kim et al. [65] and Kicir et al. [66].

Subsequently, a third component of XPS O1s line located at 533.9 eV, evidently higher with respect to the previous one, can be attributed to the adventitious carbon dioxide O-C=O surface bondings existed at the surface of ZnO NWs.

Finally, the fourth wide component of XPS O1s line located at 534.6 eV, having the smallest amplitude, can be attributed to the carboxyl acid COOH groups adsorbed at the surface ZnO nanostructures. The similar component(s) were observed for ZnO thin films by Lupan et al. [61], and for the porous ZnO single crystals by Yao et al. [67].

Only three among the above mentioned XPS O1s line components are clearly visible after the TPD process. Apart from the main XPS O1s component located at 531.2 eV attributed to the presence of partially reduced ZnO as ZnO_x and directly related to the existence of O_2^- ions in the oxygen-deficient regions, there are two XPS O1s components related to existence of surface contaminations at

the surface of ZnO NWs. As before, a second component of XPS O1s line located at 532.8 eV, evidently lower in intensity, can be attributed to the presence of adsorbed hydroxyl groups. A third wide component of XPS O1s line located at 534.6 eV, having the smallest amplitude, is also observed, which can be attributed to the carboxyl acid COOH groups adsorbed at the surface ZnO nanostructures.

What is crucial after TPD process the XPS O1s line component at the binding energy of 533.9 eV, attributed to the adventitious carbon dioxide O-C=O surface bondings is not observed. This is probably related to the fact that during the TPD process there is an evident desorption of C contaminations in form of CO_2, causing an increase of the contribution from loosely bounded oxygen in adsorbed hydroxyl groups. These information on the behaviour of XPS O1s components are in good correlation with the information related to the evolution of XPS C1s peaks and their potential components presented in Figure 7.

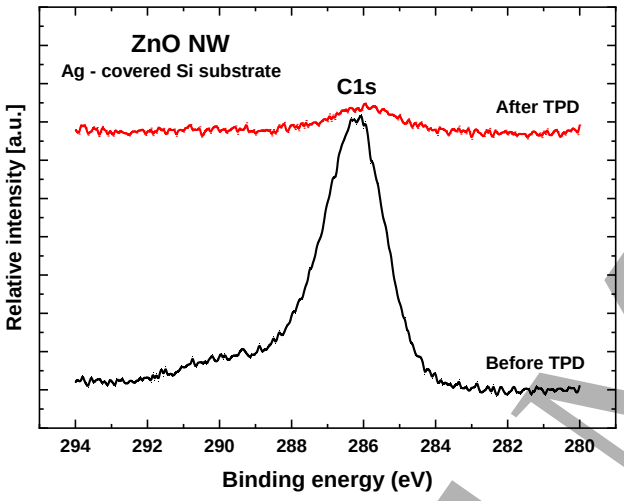

Figure 7. Evolution of XPS C1s lines for ZnO NWs before the TPD process.

As was already mentioned, after the TPD process the contribution of undesired C contaminations drastically decreased is confirmed by the fact that the signal-to-noise (S/N) ratio of XPS C1s line was at the level of 3.
Moreover, for the ZnO NWs before TPD process, contrary to XPS O1s lines, the XPS C1s line exhibits only a weak asymmetry. Nevertheless, it is surely related to the existence of chosen forms of carbon bondings at surface, which have been recognized after the deconvolution of XPS C1s lines using Gauss fitting. The obtained results are shown in Figure 8. Thanks to the deconvolution procedure, with high line fitting parameter (RMS ~ 0.98), it is evident that the XPS C1s line exhibits three components clearly visible at binding energy of 286.1 eV, 287.8 eV, and 288.8 eV, respectively.

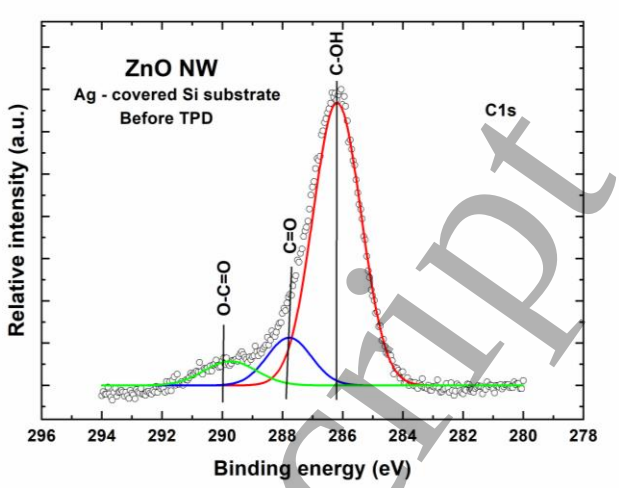

Figure 8. The XPS C1s lines for ZnO NWs before the TPD process after deconvolution using Gauss fitting (dark circles – experimental spectra; colour solid lines – respective fitted components).

The first one, which can be treated as the main peak located at 286.1 eV, can only be attributed to C-O type surface bondings such as C-OH, commonly observed at the surface of various form of oxides, in the well-known reference book [49]. This is in a good correlation with the fact that adsorbed hydroxyl groups at surface of ZnO NWs have been recognized also in the XPS O1s line(s), as mentioned. Other components (of evidently lower amplitude), located at the binding energy 287.8 eV and 288.8 eV, can be attributed to the various forms of carbon oxides bondings like C=O and O=C–O, respectively.

Because, as was mentioned above, after TPD process the signal-to-noise ratio was 3, the deconvolution procedure would be doubtful. Nevertheless, it is evident that only the main peak located at 286.1 eV can be recognized, attributed to the hydroxyl surface bondings such as C-OH. The existence of these C-OH surface bondings can strongly affect the variation of local surface chemistry of our ZnO NWs for their potential sensor application.

In addition to the above analysis, the adsorbed adventitious carbon dioxide CO_2 combined with carboxyl acid COOH groups adsorbed at the surface of our ZnO NWs have been recognized from the respective XPS O1s line at the binding energy ~ 534 eV, as for ZnO films deposited by atomic layer deposition (ALD) [68].
All the obtained XPS information on the local surface chemistry (stoichiometry/nonstoichiometry combined with undesired surface contaminations) of ZnO NWs before and after the TPD process are in good correlation with the respective information obtained by our complementary studies performer by TDS methods. The TDS spectra of main residual gases desorbed from the investigated ZnO NWs after their exposure to air atmosphere are displayed in Figure 9 which for the clarity have been additionally

corrected by the ionization probability of respected gases detected in our experiments.

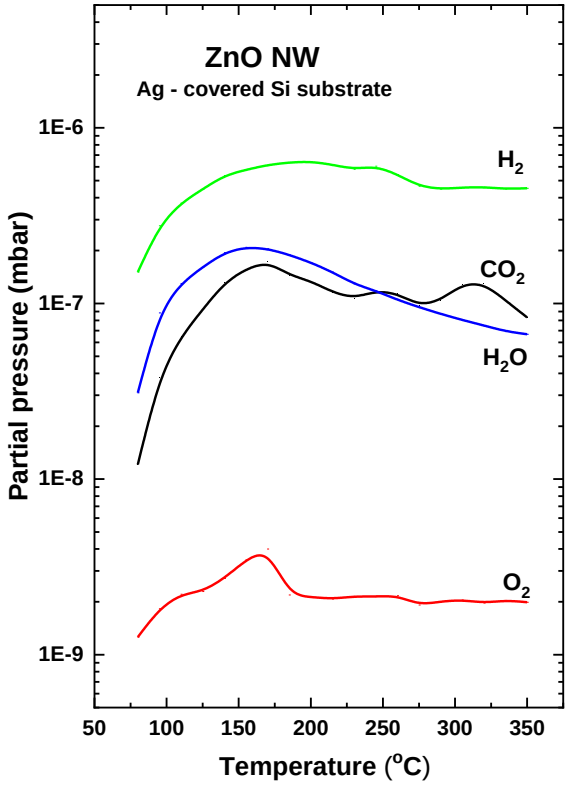

Figure 9. TDS spectra of main residual gases desorbed from the ZnO NWs exposed to air.

Based on results of our TDS studies shown in Figure 9 it is clear that mostly the molecular hydrogen (H_2) was desorbed during TPD process with the highest relative partial pressure (in the range of 10^{-6}÷ 10^{-7} mbar), starting already even below 100 °C, with an almost flat trend in the temperature range 150 ÷ 350 °C. This is probably related to the high degree of crystalline form of ZnO NWs, because such forms of the molecular hydrogen, in general, can penetrate their subsurface region, especially at lower temperature. To the best of our knowledge, this has never been reported for ZnO NWs in the available literature.

In turn, rather only a very small amount of the molecular oxygen (O_2) desorbs from our ZnO NWs at the relative partial pressure close to 10^{-9} mbar, also starting even below 100 °C and having evident maximum at about 165 °C. It means that probably the residual oxygen from air atmosphere is only physically adsorbed at the surface of ZnO NWs. Nevertheless, the relative [O]/[Zn] concentration after the TDS process only slightly decreased, as evidenced from our XPS measurements, which will be discussed later on.

At this moment it should be underlined, what is commonly known, that water vapour (H_2O), and various carbon oxides (CO_x) are the main residual gases, playing an extremely important and uncontrolled role in the gas sensing mechanism [5,6]. This is why in our TDS studies a special attention was given on the detection and analysis of these last two residual gas components.

From our TDS spectra shown in Figure 9, it is clear that H_2O desorbs from our ZnO NWs at the partial pressure in the range of 10^{-6} ÷ 10^{-7} mbar, also starting below 100°C, with a rather oscillating tendency in temperature range 150 ÷ 350°C. These oscillations correspond to the three local maxima observed at the TDS spectrum at ~ 170 °C, 250 °C, and 320 °C. It means that there are different forms of the hydroxyl groups at the surface of crystalline ZnO NWs.

In turn, the carbon oxides (CO_x), in our TDS studies only carbon dioxide CO_2 was detected, as shown in the respective TDS spectrum. The relative partial pressure also changed in the similar range of 10^{-6} ÷ 10^{-7} mbar, as for the case of H_2O desorption, starting already below 100 °C with the almost constant tendency in the temperature range of 150 ÷ 350 °C, having the maximum at about 170 °C.

In relation to the above TDS information it is clear that the effect of desorption of H_2O and CO_2 residual gases was in a quite good correlation with the variation of relative concentration of the main elements at the surface of ZnO NWs, leading to an almost complete vanishing of the various forms of carbon C contaminations, as determined in our XPS experiments.

At this moment it should be additionally underlined that thanks to the removal of C contaminations, the surface of ZnO NWs became more nonstoichiometric, what is of great importance when using our samples for the detection of oxidizing gases [5,6]. It directly confirms the possibility to completely remove the C contaminations during heating processes from the surface of ZnO NWs, which can not only allows their better sensitivity, but also the shorter response/ recovery time(s), being still one of the most critical limitation of the conductometric metal oxides gas sensors even based on nanostructures, including ultrathin films and nanolayers [5,6].

Conclusions

Thanks to comparative studies, the local surface properties of ZnO nanowires deposited by evaporation-condensation method on Ag-covered Si substrate were investigated. It was shown from our SEM studies that ZnO NWs are mostly isolated and irregular, having an average length of μm and diameters at the level of tens nm. In turn, from our XPS studies it was confirmed that ZnO NWs are slightly nonstoichiometric, additionally covered by the undesired various forms of C contaminations, including C-OH species, that can be almost completely removed during the subsequent TPD process. This information is of great importance because the undesired C contaminations play the role of undesired barriers for the gas adsorption, and can

strongly affect the uncontrolled sensor ageing effect, what still remains unclear and requires additional further studies.

Acknowledgements

The work of MK, AKK and JS has been supported by the research grant of National Science Centre, Poland - OPUS 11, 2016/21/B/ST7/02244, and additionally MK would like to acknowledge the funding of Professor Grant (GP) of the Silesian University of Technology 02/030/RGP19/0050.

References

[1] Jagadish Ch., Pearton S. Zinc Oxide: Bulk, Thin Films and Nanostructures, 1st ed.; Elsevier: Amsterdam, 2006.

[2] Elmer K., Klein A., Rech B., Transparent Conductive Zinc Oxide – Basics and Application in Thin Films Solar Cells, Springer: Berlin, 2007.

[3] Özgür Ü., Hofstetter D., Morkoc H. ZnO Devices and Applications: a Review of Current Status and Future Prospects, 2010, Proc.IEEE 98 (7),1255–1268.

[4] Zhang Q., Dandeneau C.S., Zhou X., Cao G. ZnO nanostructures for dye sensitized solar cells, 2009, Adv.Mater. 21, 4087–4108.

[5] Eranna, G. Metal oxide nanostructures as gas sensing devices, CRC Press: Boca Raton, 2012

[6] Carpenter M.A., Mathur S., Kolmakov A. Metal oxide nanomaterials for chemical sensors, Springer: New York, 2012.

[7] Sberveglieri G., Nelli P., Groppelli S., Quaranta F., Valentini A., Vasanelli L. Oxygen gas sensing characteristics at ambient pressure of undoped and lithium-doped ZnO-sputtered thin films, 1990, Mater. Sci. Eng. B, 7/1-2, 63-68;

[8] Rothschild A., Komen Y. The Effect of Grain Size on the Sensitivity of Nanocrystalline Metal-Oxide Gas Sensors. 2004, J. Appl. Phys. 95, 6374-6380.

[9] Xu J., Han J., Zhang Y., Sun Y., Xie B. Studies on alcohol sensing mechanism of ZnO based gas sensors, 2008**,** Sensors and Actuators B 132, 334–339.

[10] Bai S., Hu J., Li D., Luo R., Chen A., Liu Ch.Ch., Quantum-sized ZnO nanoparticles: Synthesis, characterization and sensing properties for NO_2, 2011, J.Mater.Chem. 2, 12288-96.

[11] Patil V.L, Vanalakar S.A., Patil P.S., Kim J.H. Fabrication of nanostructured ZnO thin films based NO_2 gas sensor via SILAR technique, 2017, Sensors and Actuators B 239, 1185-1193

[12] Gu F., You D., Wang Z., Han D., Guo G. Improvement of gas-sensing property by defect engineering in microwave-assisted synthesized 3D ZnO nanostructures, 2014, Sensors and Actuators B 204, 342–350.

[13] Bai S., Guo T., Li D., Luo R., Chen A., Liu Ch.Ch. Intrinsic sensing properties of the flower-like ZnO nanostructures, 2013, Sensors and Actuators B 182, 747-754.

[14] Hosseini Z.S., Iraji zad A., Mortlezaali A. Room temperature H_2S gas sensor based on rather aligned ZnO nanorods with a flower-like structure, 2015, Sensors and Actuators B 207, 865-871

[15] Y. Song, F. Chen, Y. Zhang, S. Zhang, F. Liu, P. Sun, X. Yan, G. Lu. Fabrication of highly sensitive and selective room-temperature nitrogen dioxide sensors based on the ZnO nanoflowers, Sensors and Actuators B 287 (2019) 191-198.

[16] Agarwal S., Rai P., Gatell N.N., Llobet E., Güell F., Kumar M., Awasthi K. Gas sensing properties of ZnO nanostructures (flowers/rods) synthesized by hydrothermal method, 2019, Sensors and Actuators B 292, 24-31.

[17] Yin M., Liu S. Preparation of ZnO hollow spheres with different surface roughness and their enhanced gas sensing property, 2014, Sensors and Actuators B 197, 58–65.

[18] Zhang H.M., Xu C., Sheng P., Chen Y.J., Yu L., Li Q.H. Synthesis of ZnO hollow spheres through a bacterial template method and their gas sensing properties, 2013, Sensors and Actuators B 181, 99–103.

[19] Han B., Liu X., Xing X., Chen N., Xiao X., Liu S., Wang Y. A high response butanol gas sensor based on ZnO hollow spheres, 2016, Sensors and Actuators B, 237, 423-430.

[20] Liu Y., Dong J., Hesketh P.J., Liu M. Synthesis and gas sensing properties of ZnO single crystal flakes, 2005, J. Mater. Chem.15, 2316–2320.

[21] Kanaparthi S., Singh S.G. Chemiresistive Sensor Based on Zinc Oxide Nanoflakes for CO_2 Detection, 2019, ACS Appl. Nano Mater. 2, 700-706.

[22] Wan Q., Li H., Chen Y.J., Wang T.H., He X.L., Li J.P., Lin C.L. Fabrication and ethanol sensing characteristics of ZnO nanowire gas sensors, 2004, Appl. Phys. Lett. 84, 3654

[23] Sberveglieri G., Baratto C., Comini E., Faglia G., Ferroni M., Ponzoni A., Vomiero A. Synthesis and characterization of semiconducting nanowires for gas sensing, 2007, Sensors and Actuators B 121, 208–213.

[24] Lupan O., Emelchenko G.A., Ursaki V.V., Chai G., Redkin A.N., Gruzintsev A.N., Tiginyanu I.M., Chow L., Ono L.K., Roldan Cuenya B., Heinrich H., Yakimov E.E. Synthesis and characterization of ZnO nanowires for nanosensor applications, 2010, Materials Research Bulletin 45, 1026–1032.

[25] Huang, H.; Xu, P.; Zheng, D.; Chen, C.; Li, X. Sulfuration–desulfuration reaction sensing effect of intrinsic ZnO nanowires for high-performance H_2S detection. 2015, J. Mater. Chem. A 3, 6330–6339.

[26] Huber F., Riegert S., Madel M., Thonke K. H_2S sensing in ppb regime with zinc oxide nanowires, 2017, Sensors and Actuators B, 239, 358-363.

[27] Vardan G., Poli N., Comini E. Highly Sensitive and Selective H_2S Chemical Sensor Based on ZnO Nanomaterial. 2019, Appl. Sci. 9, 1167.

[28] Wang C., Chu X., Wu M. Detection of H_2S down to ppb levels at room temperature using sensors based on ZnO nanorods, 2006, Sensors and Actuators B, 113, 320–323.

[29] Cho P.S., Kim K.W., Lee J.H. NO_2 sensing characteristics of ZnO nanorods prepared by hydrothermal method, 2006, J.Electroceram. 17, 975–978.

[30] Wang L., Kang Y., Liu X., Zhang S., Huang W., Wang S., ZnO nanorod gas sensor for ethanol detection, 2012, Sensors and Actuators B 162, 237–243.

[31] Shaikh S.K., Ganbavale V.V., Mohite S.V., Patil U.M., Rajpure K.Y. ZnO nanorod based highly selective visible blind ultra-violet photodetector and highly sensitive NO_2 gas sensor, 2018, Superlattices and Microstructures 120, 170-186.

[32] Labis J.P., Al-Anazi A.Q., Al-Brithen H.A., Hezam M., Alduraibi M.A., Algarni A., Alharbi A.A., Al-Awadi A.S., Khan A., El-Toni A.M. Designing zinc oxide nanostructures

(nanoworms, nanoflowers, nanowalls, and nanorods) by pulsed laser ablation technique for gas-sensing application, 2019, J. Am. Ceram. Soc. 102, 4367–4375.

[33] Jin X.-B., Li Y.-X., Su Y., Guo Z., Gu C.-P., Huang J.-R., Meng F.-L., Huang X.-J., Li M.-Q., Liu J.-H. Porous and single-crystalline ZnO nanobelts: fabrication with annealing precursor nanobelts, and gas-sensing and optoelectronic performance, 2016, Nanotechnology 27, 355702.

[34] Kaur M., Kailasaganapathi S., Ramgir N., Datta N., Kumar S., Debnath A.K., Aswal D.K., Gupta S.K. Gas dependent sensing mechanism in ZnO nanobelt sensor, 2017, Applied Surface Science 394, 258–266.

[35] Kolmakov A., Moskovits M. Chemical sensing and catalysis by one-dimensional metal-oxide nanostructures, 2004, Ann. Rev. Mater. Res. 34, 151–180.

[36] Lu J.G., Chang P., Fan Z. Quasi-one-dimensional metal oxide materials: synthesis, properties and applications, 2006, Mater. Sci. Eng. Rep. 52, 49–91.

[37] Comini E., Baratto C., Faglia G., Ferroni M., Vomiero A., Sberveglieri G. Quasi one dimensional metal oxide semiconductors: preparation, characterization and application as chemical sensors, 2009, Prog. Mater. Sci. 54, 1–67.

[38] Zhang Y., Ram M.K., Stefanakos E.K., Goswami D.Y. Synthesis, Characterization, and Applications of ZnO Nanowires, 2012, Journal of Nanomaterials - Article ID 624520, 22 pages.

[39] Galstyan V., Comini E., Ponzoni A., Sberveglieri V., Sberveglieri G. ZnO Quasi-1D Nanostructures: Synthesis, Modeling, and Properties for Applications in Conductometric Chemical Sensors, 2016, Chemosensors 4, 1-21.

[40] Rackauskas S., Barbero N., Barolo C., Viscardi G. ZnO Nanowire Application in Chemoresistive Sensing: A Review 2017, Nanomaterials 7, 381.

[41] Leonardi S.G. Two-Dimensional Zinc Oxide Nanostructures for Gas Sensor Applications, 2017 Chemosensors 5 ,17.

[42] Allen M.W., Swartz C.H., Myers T.H., Veal T.D., McConville C.F., Durbin S.M. Bulk transport measurements in ZnO: The effect of surface electron layers, 2010, Phys. Rev.B 81, 075211.

[43] Kaciulis S., Pandolfi L., Comini E., Faglia G., Ferroni, M., Sberveglieri G., Kandasamy S., Shafiei M., Wlodarski M. Nanowires of metal oxides for gas sensing applications, 2008, Surface and Interface Analysis 40, 575–578

[44] Waclawik E.R., Chang J., Ponzoni A., Concina I., Zappa D., Comini E., Motta N., Faglia G., Sberveglieri G. Functionalised zinc oxide nanowire gas sensors: Enhanced NO_2 gas sensor response by chemical modification of nanowire surfaces, 2012, Beilstein Journal of Nanotechnology 3, 368-377

[45] Kwoka M., Lyson-Sypien B., Kulis A., Maslyk M., Borysiewicz M.A., Kaminska L., Szuber J. Surface properties of nanostructured porous ZnO thin films prepared by direct current reactive magnetron sputtering, 2018, Materials, 11, 131.

[46] Sitarz M., Kwoka M., Comini E., Zappa D., Szuber J. Surface chemistry of the SnO_2 nanowires on Ag catalyst-covered Si substrate studied by XPS and TDS methods, 2014, Nanoscale Research Letters 9, 43, pp.6

[47] Kwoka M., Ottaviano L., Koscielniak P., Szuber J. XPS, TDS and AFM studies of surface chemistry and morphology of Ag-covered L-CVD SnO_2 nanolayers, 2014, Nanoscale Research Letters 9, 260, 9 pp.

[48] Wagner C.D., Riggs W.M., Davis L.E., Moulder J.F., Mnilenberger G.E. Handbook of X-ray Photoelectron Spectroscopy, Perkin-Elmer: Eden Prairie, MN, 1979

[49] Moulder J.F., Chastain J. Handbook of X-ray photoelectron spectroscopy: a reference book of standard spectra for identification and interpretation of XPS data, (Eds.), Perkin-Elmer Corp: UK, 1995.

[50] Hoflund G., Epling W.S., Minaham D.M. Surface characterization study of a 1 wt% K-promoted ZnO, higher alcohol synthesis catalyst, 1998, Journal of Electron Spectroscopy and Related Phenomena, 95 (2-3), 289–297.

[51] Thompson A., Vaughan D. X-Ray Data Booklet-Center for X-Ray Optics and Advanced Light Source, 2nd ed., Berkeley: California, 2001.

[52] Ikeo N., Iijima Y., Nimura N., Sigematsu M., Tazawa T., Matsumoto S., Kojima K., Nagasawa Y. Handbook of X-ray Photoelectron Spectroscopy, JEOL, 1991.

[53] Archana J., Navaneethan M., Hayakawa Y. Morphological transformation of ZnO nanoparticle to nanorods via solid-solid interaction at high temperature annealing and functional properties, 2016, Scr. Mater 113, 163-166.

[54] Guo L., Yang S.H. Highly monodisperse polymer-capped ZnO nanoparticles: Preparation and optical properties, 2000, Appl. Phys. Lett. 76, 2901-2903.

[55] Armelao L., Fabrizio M., Gialanella S., Zordan F. Sol–gel synthesis and characterization of ZnO-based nanosystems, 2001, Thin Solid Films 394, 90-96.

[56] Chen M., Wang X., Yu Y.H., Pei Z.L., Bai X.D., Sun C., Huang R.F., Wen, L.S. X-ray photoelectron spectroscopy and auger electron spectroscopy studies of Al-doped ZnO films, 2000, Appl. Surf. Sci. 158, 134–140.

[57] Kaneva N., Stambolova I., Blaskov V., Dimitriev Y., Bojinova A., Dushkin C. A comparative study on the photocatalytic efficiency of ZnO thin films prepared by spray pirolysis and sol–gel method, 2012, Surf. Coat. Technol 207, 5–10.

[58] Li L.J., Deng H., Dai L.P., Chen J.J., Yuan Q.L., Li Y. Properties of Al heavy doped ZnO thin films by RF magnetron sputtering, 2008, Mater. Res. Bull. 43, 1456–1462.

[59] Chen M., Wang Z., Han D., Gu F., Guo G. High-sensitivity NO_2 gas sensors based on flower-like and tube-like ZnO nanomaterials, 2011, Sensors and Actuators B 157, 565–574.

[60] Hsieh P.T., Chen Y.C., Kao K.S., Wang C.M. Luminescence mechanism of ZnO thin film investigated by XPS measurement, 2008, Appl Phys. A, 90, 317.

[61] Lupan O., Pauporte T., Chow L., Viana B., Pelle F., Ono L.K., Cuenya B.R., Heinrich H. Effects of annealing on properties of ZnO thin films prepared by electrochemical deposition in chloride medium, 2010, Appl. Surf. Sci. 256, 1895-1907.

[62] Stambolova I., Blaskov V., Shipochka M., Vassilev S., Petkova V., Loukanov A. Simple way for preparation of ZnO films by surfactant mediated spray pirolysis, 2012, Materials Science and Engineering B 177, 1029–1037.

[63] Lee J., Chung J., Lim S. Improvement of optical properties of post- annealed ZnO nanorods, 2010, Physica 42(8), 2143–2146.

[64] Bai S., Hu J., Li D., Luo R., Chen A., Liu Ch.Ch. Quantum-sized ZnO nanoparticles: Synthesis, characterization and sensing, properties for NO_2. 2011, J. Mater. Chem. 21, 12288–12294.

[65] Kim W., Choi M., Yong K. Generation of oxygen vacancies in ZnO nanorods/films and their effects on gas sensing properties, 2015, Sensors and Actuators B 209, 989–996.

[66] Kıcır N., Tüken T., Erken O., Gumus C., Ufuktepe Y. Nanostructured ZnO films in forms of rod, plate and flower: Electrodeposition mechanisms and characterization, 2016, Applied Surface Science 377, 191–199.

[67] Yao M., Ding F., Cao Y., Hu P., Fan J., Lu Ch., Yuan F., Shi Ch., Chen Y. Sn doped ZnO layered porous nanocrystals with hierarchical structures and modified surfaces for gas sensors, 2014, Sensors and Actuators B 201, 255–265.

[68] Drozd V.E., Titov V.V., Kasatkin I.A., Basov L.L., Lisachenko A.A., Stroyuk O.L., Kuchmiy S.Y. Structure, optical properties and visible-light-induced photochemical activity of nanocrystalline ZnO films deposited by atomic layer deposition onto Si(100), 2014, Thin Solid Films 573, 128–133.